CMOS Skin Sensor for Mobile Skin Diagnosis Using an Electronic Cotton Pad

HYUNSUB NORBERT RIE[1], (Member, IEEE), JUNHYUNG CHO[1], (Member, IEEE), JUNGJOON LEE[2],
SRINIVAS GANDLA [2], SEONG-JIN KIM [3], (Member, IEEE),
AND JAEHYUK CHOI [1], (Member, IEEE)

[1]College of Information and Communication Engineering, Sungkyunkwan University, Suwon 16419, South Korea
[2]Department of Advanced Materials and Science Engineering, Sungkyunkwan University, Suwon 16419, South Korea
[3]School of Electrical and Computer Engineering, Ulsan National Institute of Science and Technology, Ulsan 44919, South Korea

Corresponding authors: Jaehyuk Choi (choix215@skku.edu) and Seong-Jin Kim (kimsj@unist.ac.kr)

ABSTRACT This paper presents a complementary metal–oxide semiconductor (CMOS) skin sensor for detecting hydration, sebum, and ultraviolet (UV) protection. This sensor employs pixels comprising interdigitated capacitors (IDCs) for detecting hydration and a 30×24 photodiode (PD) array for detecting UV protection and sebum. The 4×8 pixels with IDCs over the PDs are used for area efficiency; they afford reliable detection regardless of the skin contact area and a high sensitivity, which is achieved via pixel merging. For the readout of both IDCs and PDs, a column-parallel multiple-sampling analog front-end and a 9b successive approximation register analog-to-digital converter are integrated. To detect UV protection under different wavelengths of UV_A and UV_B, we implement the spatiotemporal delta readout of the PDs. Furthermore, a fully characterized, proof-of-concept prototype chip is fabricated using a 110-nm CMOS process. Compared with conventional skin sensors, the proposed sensor exhibits higher sensitivities of 0.25%/min and 2.32%/mL in detecting dehydration rate and sebum levels, respectively. Moreover, the sensor can detect UV protection under UV_A and UV_B wavelengths. Owing to its core size of 2.32×4.65 mm^2, the proposed sensor can potentially be integrated into cotton pads for mobile skin diagnosis.

INDEX TERMS Biosensors, CMOS, hydration, sebum, skin, ultraviolet protection.

I. INTRODUCTION

Owing to the currently increasing emphasis on skin care, there has been an increase in the demand for mobile approaches enabling the detection and evaluation of skin hydration and sebum levels, as well as ultraviolet (UV) protection. However, the use of skin sensors has been limited to dermatological diagnosis [1]–[3] or cosmetic applications because of their considerable size and cost. The emphasis on skincare has promoted the commercialization of several portable devices [4]–[7], including devices featuring built-in Bluetooth transceivers for transmitting skin statuses, such as hydration and sebum levels, to mobile devices for diagnosis. However, their large form factors (>25 cm^3) and high costs ($>\$100$) have impeded their widespread application. Moreover, these devices also require significant amounts of power (>250 mW), thereby necessitating additional space

The associate editor coordinating the review of this manuscript and approving it for publication was Yiming Huo .

for batteries. Most importantly, these sensors exhibit low sensitivity in detecting significant changes in hydration and sebum levels; the functionality of these devices is also limited as they are only capable of measuring two types of skin statuses, i.e., hydration and sebum, and not UV protection.

To measure skin hydration, a large, external interdigitated capacitor (IDC) needs to be connected to discrete integrated circuits for measuring changes in permittivity based on skin moisture [4], [7], [8]. However, such sensor devices cannot be miniaturized owing to the off-chip IDC. Additionally, separate photodetectors are required, which increases the cost and area of the sensor system. Although bioimpedance analysis can be used to measure hydration, the accuracy of this approach is lower than that of capacitance measurements [8].

Apart from moisture and sebum, detecting UV protection is also important because overexposure to UV light can result in sunburns as well as skin cancer [10]–[12]. According to its wavelength (λ), UV light can be classified as UV_A (320–400 nm), UV_B (280–320 nm), and UV_C (200–280 nm).
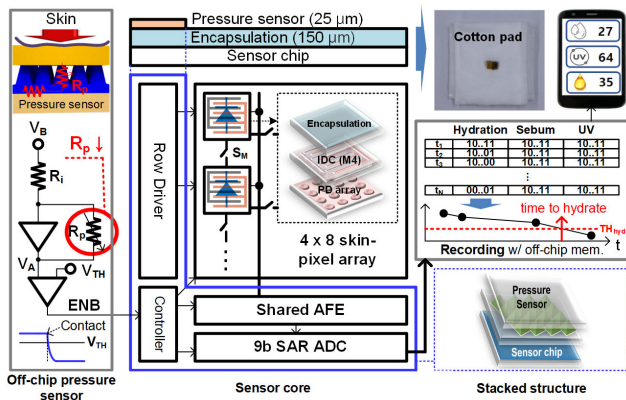
FIGURE 1. Architecture of proposed CMOS skin sensor for mobile skin diagnosis integrated on an electronic cotton pad.

The ozone layer absorbs most of UV_C entering the Earth's atmosphere; however, UV_A and UV_B pass through the ozone layer and lead to different harmful effects on skin. UV_A leads to skin tanning and induces long-term skin damage that contributes to skin aging; in contrast, UV_B leads to skin burns and induces skin cancer. Although a few conventional skin sensors can measure UV radiation based on sunlight [6], these sensors cannot distinguish between UV_A and UV_B; more importantly, they do not account for the UV protection afforded by sunblock that is already applied to the skin.

This paper presents a complementary metal–oxide semiconductor (CMOS) skin sensor that measures the skin hydration, sebum, and UV protection for mobile skin diagnosis. Using a CMOS process, the sensor could be miniaturized to <9 mm^2, enabling its integration in a cotton pad. It also features 4 × 8 skin pixels that allow for reliable detection regardless of the skin contact area as well as high sensitivity, which is achieved using pixel merging. Each pixel comprises IDCs stacked on a 30 × 24 photodiode (PD) array for area efficiency. To detect UV protection against different wavelengths (i.e., UV_A and UV_B), we employed the spatiotemporal delta (Δ) readout of the PDs. For the readouts of the IDCs and PDs, a column-parallel multiple-sampling analog front-end (AFE) and 9b successive approximation register (SAR) analog-to-digital converter (ADC) were integrated. Owing to a core size of 2.32 × 4.65 mm^2, the proposed sensor can be integrated into a cotton pad for mobile skin diagnosis.

The remainder of this paper is organized as follows. Section II presents the sensor architecture and detection principles for each skin parameter. Section III focuses on the readout circuits. The experimental results are presented in Section IV, while Section V highlights the conclusions of this research.

II. SENSOR ARCHITECTURE AND DETECTION PRINCIPLES
The architecture of the proposed sensor is shown in Fig. 1. This sensor employs 4 × 8 pixels to detect the local statuses of skin. Each pixel consists of a top metal layer (metal-4) IDC for detecting hydration and an n$^+$/p-sub PD array for detecting UV protection and sebum. The PD array is placed under

the exposed portion of the IDC to collect incident photons. Charges from both the IDC and the PD are provided to the column-parallel shared AFE and 9b SAR ADC at different times. The chip is covered with glass to generate a constant electric field (e-field) in skin as well as for encapsulation.

Above the glass, a resistive pressure sensor with a pyramid microstructure [13] is partially stacked for detecting skin contact (indicated by a 30-fold decrease in resistance under a pressure of 13 kPa) as well as for awakening (ENB = 0) the sensor from its sleep mode. The pressure sensor is stacked on the encapsulated portion, i.e., the blue square in Fig. 1, such that it does not block incident light. The resistance (R_p) of the polydimethylsiloxane-based pyramid microstructure coated with a conducting polymer varies with respect to the applied pressure. On increasing the pressure, R_p is reduced, and the off-chip resistive feedback amplifier produces a diminished output upon skin contact. By comparing the amplifier output (V_A) with the reference voltage V_{TH}, the signal ENB triggers the sensor upon skin contact. The analog output V_A of the amplifier is converted into a digital signal via the off-chip ADC. This digital signal of the contact pressure is continuously recorded and utilized to select an appropriate sensor output that is generated under a specific contact pressure. During measurements, we successively captured >100 samples when the sensor was in contact with skin. Additionally, multiple outputs of the external ADC, which digitized V_a, were captured. These two capturing operations were synchronized. We predefined the range of the ADC output, i.e., the effective range of contact pressure. To acquire appropriate outputs from multiple samples, a sample with an ADC output close to the median of the predefined range was selected. Therefore, the sensor output is deemed reliable for acquiring detection results under a constant contact pressure.

The measured skin statuses were chronologically recorded in the off-chip memory for long-term monitoring of skin, as shown in Fig. 1. The graph shows an example of the hydration level over time. After the application of moisturizing cream, the skin moisture continuously decreased owing to natural dehydration and finally approached the threshold value, indicating that rehydration was necessary.

The detection principle of the proposed sensor is illustrated in Fig. 2. To measure hydration, the change in permittivity with respect to skin moisture is detected. Specifically, the change in capacitance is evaluated for measuring the change in permittivity. Skin moisture resides in the stratum corneum, which has a thickness of 60 μm. For accurate detection of hydration, the e-field penetrating the stratum corneum should be sufficiently strong to detect even small amounts of moisture. Accordingly, the dimensions of the IDC should be carefully selected. As the thickness of the metal-4 could not be altered and the thickness of glass was predetermined to be 150 μm, we optimized the width (W) and distance (D) such that a strong e-field was generated in the range of 150–210 μm (i.e., in the stratum corneum) from the metal-4. For optimization, we performed e-field simulations using Maxwell 3D and determined the optimal value of W
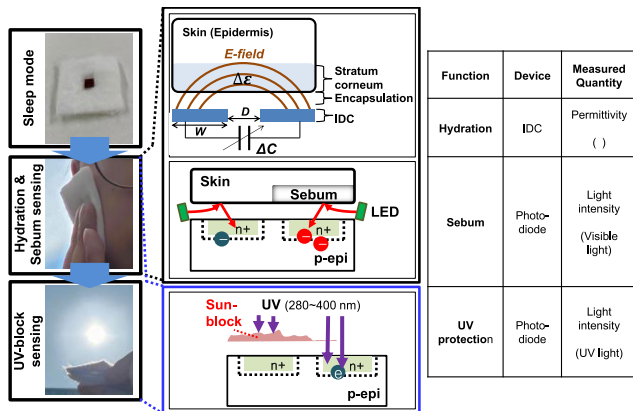
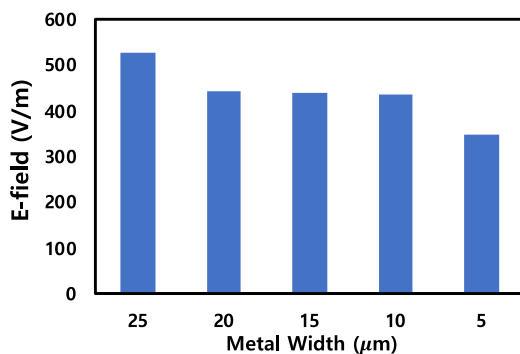**FIGURE 2.** Operation principles of hydration sensing (top), sebum sensing (mid), and UV-block sensing (bottom).

FIGURE 3. Simulation results for IDCs: averaged e-field in the stratum corneum (150–210 μm from the top metal layer) for different values of W.

and D to be 25 and 50 μm, respectively. Fig. 3 shows the simulation results for the e-field in the range of 150–210 μm from the metal-4 (i.e., in the stratum corneum); the graph shows the averaged values of the e-field in this range. Here, W + D is fixed at 75 μm, and the change in the e-field with respect to W is presented. The maximum e-field in the stratum corneum was generated when W was set as 25 μm. The area of the IDC is also an important factor affecting sensitivity. This area was set as 375×500 μm^2, to ensure that the 30×24 PD array with a unit size of 3.6×3.6 μm^2 could be accommodated in a single IDC. The PDs were located only in the aperture of the IDC. Even if the e-field from one IDC is weak, a stronger e-field is generated by the sum of the e-fields from multiple IDCs [14], [15]. We placed inter-IDC switches (S_M) to connect neighboring IDCs, as shown in Fig. 1. The number of IDCs to be merged can be modified to alter the pixel resolution of 4×8 into 2×8, 1×2, or 1×1. When multiple IDCs are connected, the sum of charges from multiple IDCs is transferred to a small feedback capacitance in the capacitive feedback amplifier of the shared AFE. The detailed operation of this amplifier is presented in Section III. Thus, sensitivity can be intentionally increased by merging multiple pixels, even though a single IDC has a fixed area of 375×500 μm^2.
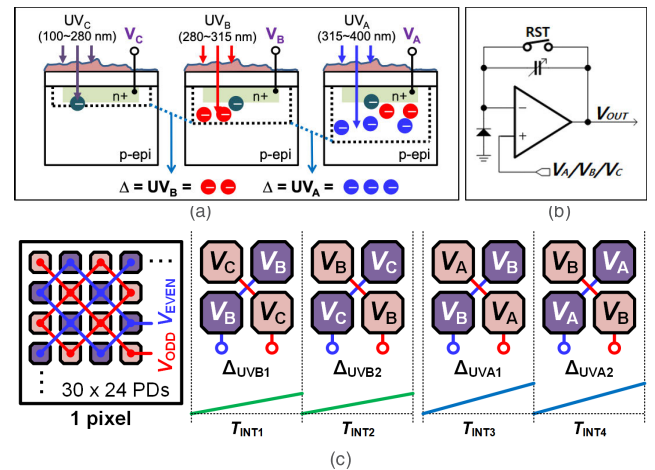

FIGURE 4. Spatiotemporal Δ-readout for UV measurement: (a) principle of Δ-readout with variable reset voltages; (b) active reset with AFE circuit; (c) spatiotemporal Δ-readout.

For sebum detection, the in-pixel PDs detect light reflected from skin using a visible light-emitting diode (LED). Oily skin with sebum reflects a greater amount of light. Therefore, the amount of sebum can be determined by measuring the number of photogenerated electrons in the PDs.

The in-pixel PDs also detect UV protection by measuring the decrement in light intensity. For measuring these decrements, PDs are used to measure the intensity of light penetrating the sunblock that is transferred from the skin. The amount of sunblock on the skin continuously decreases over time. When the sensor is contacted with the skin to transfer sunblock to the glass after a specific time, the transferred sunblock on the glass has weakened UV protection capability. Therefore, by measuring the amount of UV radiation penetrating the glass, we can indirectly measure the UV protection capability at any specific time. In the proposed approach, hydration and sebum are detected when the sensor is in contact with skin, whereas UV protection is evaluated based on the transferred sunblock on the glass (which is transferred from the skin).

For distinguishing between different λs (i.e., UV$_A$ and UV$_B$) and their harmful effects, we propose the spatiotemporal Δ-readout, as shown in Fig. 4(a). The basic principle of separating different λs is based on the image sensor reported in [16], which generates triple depletion regions in a PD for separating RGB light. In the proposed sensor, spatiotemporally varying reset voltages are used to separate UV$_A$ and UV$_B$. Neighboring pixels are reset with different voltages (V$_C$ and V$_B$ or V$_B$ and V$_A$) using a charge amplifier circuit that is shown in Fig. 4(b) in order to generate differential depletion depths. By acquiring the Δ-signals from two neighboring pixels, electrons generated in a specific λ range can be detected, because the penetration depth of photons is proportional to their λ. To eliminate spatial variations, we implement one pixel with 30×24 PDs. To apply spatiotemporal variable reset voltages and obtain Δ signals, both reset and signal lines were used to connect the PDs diagonally as illustrated

in Fig. 4(c). The integration time is divided into four parts: T_{INT1}–T_{INT4}. At T_{INT1}, UV_B is detected by using the reset voltages V_C and V_B applied to the odd and even pixels, respectively. The Δ_{UVB1} signal—a differential output of the even and odd pixels—is temporarily stored in the off-chip memory. At T_{INT2}, UV_B is detected again; however, the reset voltages (V_B and V_C) are exchanged to reduce the effects of spatial variation. Thereafter, the new Δ_{UVB2} signal from T_{INT2} is added to the previous Δ_{UVB1} signal in the off-chip memory. In a similar manner, at T_{INT3} and T_{INT4}, UV_A is detected using the reset voltages V_A and V_B.
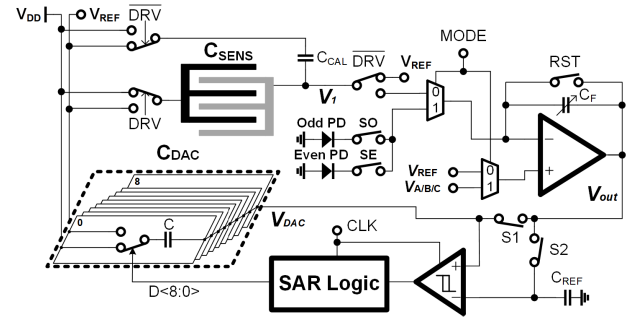
III. READOUT CIRCUITS

Fig. 5(a) presents the readout circuit, including the AFE and SAR ADC circuits. The readout circuit supports two modes: IDC readout for detecting hydration and PD readout for detecting UV protection and sebum. Using the control signal (MODE) from multiplexers, the readout circuit alters the configuration based on requirements of a specific mode.

As shown in Fig. 5(b), the IDC readout (MODE = 0) is divided into two phases: amplification and analog-to-digital conversion. The main objective of the IDC readout is to measure C_{SENS}, which includes both the intrinsic IDC capacitance (fixed) and skin capacitance (which varies with respect to the amount of moisture). For a wide range of detection, we use a calibrated capacitance C_{CAL} to detect $C_{SENS}-C_{CAL}$ instead of C_{SENS}; this is done to eliminate the large offset arising from the intrinsic IDC capacitance. C_{CAL} can be adjusted using a 4b digital signal to achieve a lower capacitance than the IDC. Fig. 5(c) shows the equivalent circuit of the amplification phase. For the IDC readout, we implemented multiple sampling to obtain an accumulated analog output via multiple measurements. For multiple sampling, the signal DRV is activated N times. During each activation, a negative step voltage drives C_{SENS}, and a positive step voltage drives C_{CAL}. Consequently, the difference in charges, i.e., charges in $C_{SENS}-C_{CAL}$, is transferred to C_F multiple times. The final output voltage is sampled in C_{REF}. The output voltage V_{out} is given as follows:

$$V_{out} = V_{REF} + N \cdot \frac{C_{SENS} - C_{CAL}}{C_F} \cdot (V_{DD} - V_{REF}). \quad (1)$$

The second phase of the IDC readout is the ADC phase, where the sampled V_{out} in C_{REF} is compared with V_{DAC} for the 9b SAR ADC.

After the IDC readout, the PD readout is initialized. A timing diagram and an equivalent circuit of the PD readout are presented in Fig. 5(d) and (e), respectively. For a simplified illustration, only the readout at T_{INT1} is depicted in Fig. 5(d). As discussed in Section II, UV_B is detected using the reset voltages of V_C and V_B at T_{INT1}. V_C is lower than V_B to ensure a differential depletion depth, as shown in Fig. 4(a). The operation consists of four phases. In the Amp1 phase, odd PDs are accessed by the charge amplifier, which generates $V_C + \Delta V_{PD(ODD)}$ by transferring charges from odd PDs. This V_{out} is sampled in C_{REF}. To acquire $\Delta V_{PD(ODD)}$,
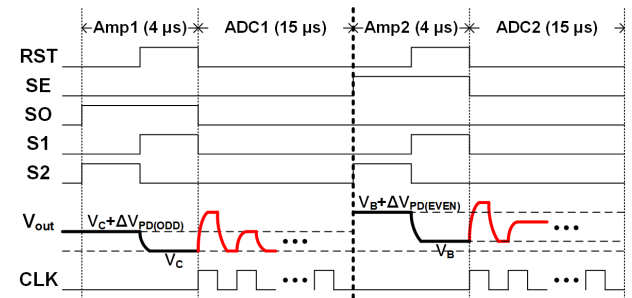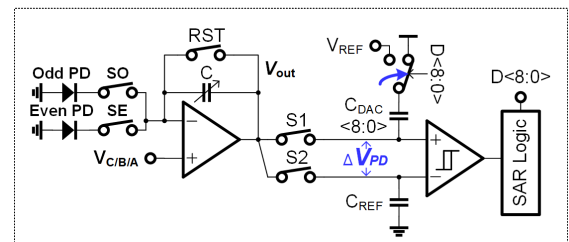

(a)
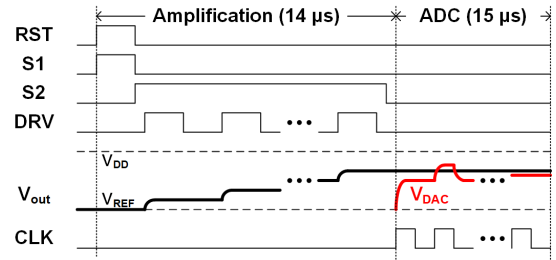
(b)
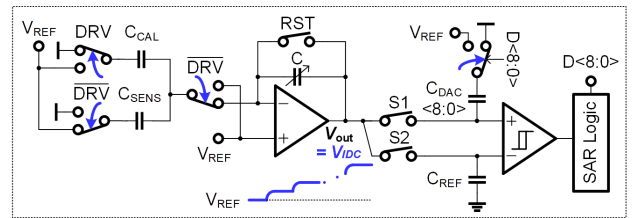
(c)

(d)

(e)

FIGURE 5. Shared AFE and SAR ADC circuits: (a) architecture; (b) timing diagram of IDC readout; (c) equivalent circuit of IDC readout; (d) timing diagram of PD readout; (e) equivalent circuit of PD readout.

the charge amplifier is reset using the unity-gain feedback. This reset voltage V_C is sampled in C_{DAC}. In the ADC1 phase, $\Delta V_{PD(ODD)}$ is converted into a 9b digital signal and tem-
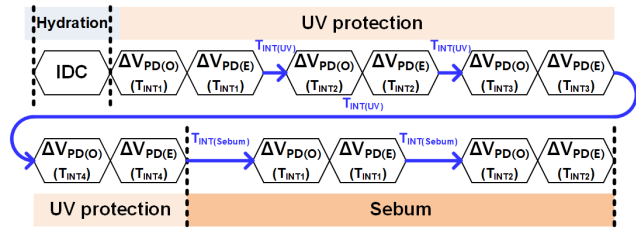
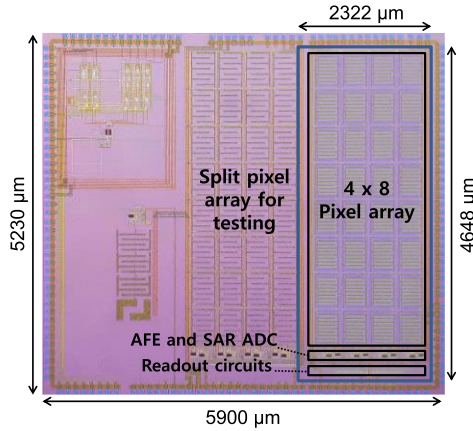**FIGURE 6.** Overall timing diagram for detection using the proposed method.

**FIGURE 7.** Chip photograph.

porarily stored in the buffer memory. In the Amp2 phase, the "+" input of the charge amplifier is converted into V_B via an off-chip digital-to-analog converter (DAC). Subsequently, the even pixels are accessed to generate $V_B + \Delta V_{PD(EVEN)}$. Thereafter, V_B is generated using the unity-gain feedback. In the ADC2 phase, a 9b digital code of $\Delta V_{PD(EVEN)}$ is generated. To acquire the Δ_{UVB} signal, the two digital codes—$\Delta V_{PD(ODD)}$ and $\Delta V_{PD(EVEN)}$—are subtracted in the off-chip processing unit.

It should be noted that similar circuit configurations and operations are used for the detection of UV protection and sebum. The only difference is that the reset voltages $V_{A/B/C}$ are provided at different timings using an off-chip DAC. For detecting UV protection, three different reset voltages are required for different λ ranges. However, for sebum detection, only two reset voltages are required for detecting a single λ (630 nm) from a red LED. As the penetration depth of UV light is low, low reset voltages are used for detecting UV protection.

Fig. 6 shows a timing diagram of the overall detection. As the three detection processes share the AFE and SAR ADC, the detections need to be performed at different timings. Moreover, the PD requires an additional integration time to accumulate incident photons, in which $T_{INT(UV)}$ is used for detecting UV protection and $T_{INT(sebum)}$ is used for detecting sebum. As sebum detection is performed for a single λ, only two integrations are required for the Δ readout; in contrast, four integrations are required for detecting UV protection.
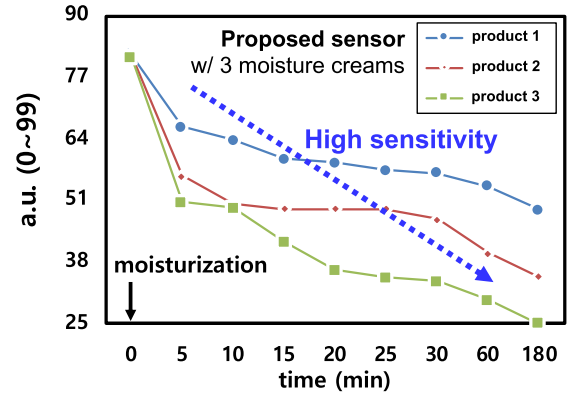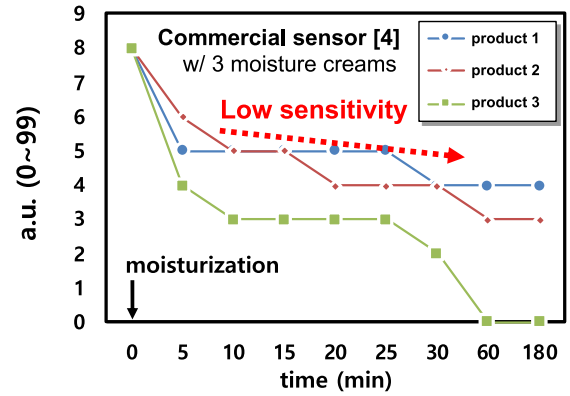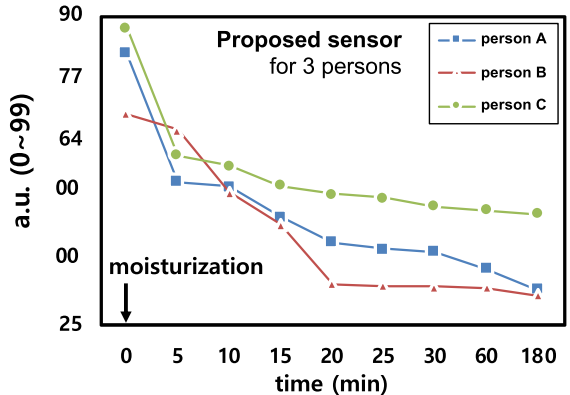
FIGURE 8. Measured skin hydration over time after the application of moisturizing creams: (a) hydration using three different moisturizing creams (products 1, 2, and 3); (b) comparison with a commercial skin sensor; (c) hydration measured from three different persons using one moisturizing cream (product 1).

IV. EXPERIMENTAL RESULTS

Fig. 7 presents a photograph of the sensor chip prototype fabricated using a 110-nm CMOS process. Excluding the split pixel array for testing purposes, the core size was 2.42×4.65 mm^2.

Fig. 8(a) shows the measured hydration over time after the application of three different moisturizing creams. The curve represents the summed results for the 2×6 IDC array, excluding peripheral pixels. This summation was performed using the 12 outputs of ADCs via an off-chip
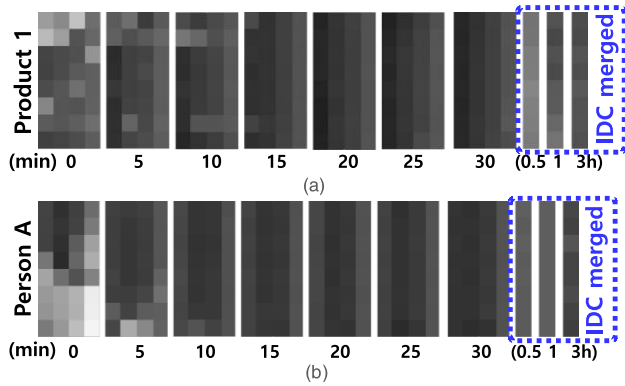
FIGURE 9. Captured images: captured images corresponding to the results for product 1 shown in Fig. 8(a); (b) captured images corresponding to the measured results for person A shown in Fig. 8(c).

processing unit. The high-end product (product 1) exhibited a superior moisturizing ability compared to the other two products. We repeated the measurements employing a commercial skin sensor used for dermatological diagnosis [4], as shown in Fig. 8(b). The results indicate that, for all the time intervals, the proposed exhibited a higher sensitivity than the commercial sensor in terms of detecting the decrement.

The quantity measured using the proposed sensor was expressed in an arbitrary unit (a.u.) for direct comparison with those measured using the commercial sensor, which yielded decimal results in the range of 0–99. The digital code (ADC output) of 511 was expressed as 99 for the comparison, as correlation between the two experiments, shown in Fig. 8(a) and (b), was important. With regard to the correlation, the proposed sensor as well as the commercial sensor [4] employed IDCs to measure the change in permittivity, although the commercial sensor used an off-chip IDC. Additionally, the same moisturizing cream and persons were used for the experiment. In the experiment, the amount of moisturizing cream was controlled using an electronic scale to ensure that the same amount of cream was applied during each measurement. However, it should be noted that the skin contact pressures were not identical, which can be attributed to human error. In the proposed sensor, an external pressure sensor ensures a relatively constant pressure during each measurement. However, the commercial sensor does not support pressure monitoring. Regardless of this error, we investigated the tendency of the decrease in moisture over time, as shown in Fig. 8(b). The results confirmed that the proposed sensor exhibits higher sensitivity than the commercial sensor.

We also measured the hydration over time for three persons using the same moisturizing cream. As shown in Fig. 8(c), the three subjects exhibited different results for hydration and its decrement, even though the same moisturizing cream was used. Hydration images were captured using the 4 × 8 IDC array, as depicted in Fig. 9. After 30 min, the pixels yielded lower values owing to the natural dehydration of skin. However, by merging pixels using inter-IDC switches (SM), sensitivity was increased sufficiently, thereby enabling the measurement of hydration even after 3 h.
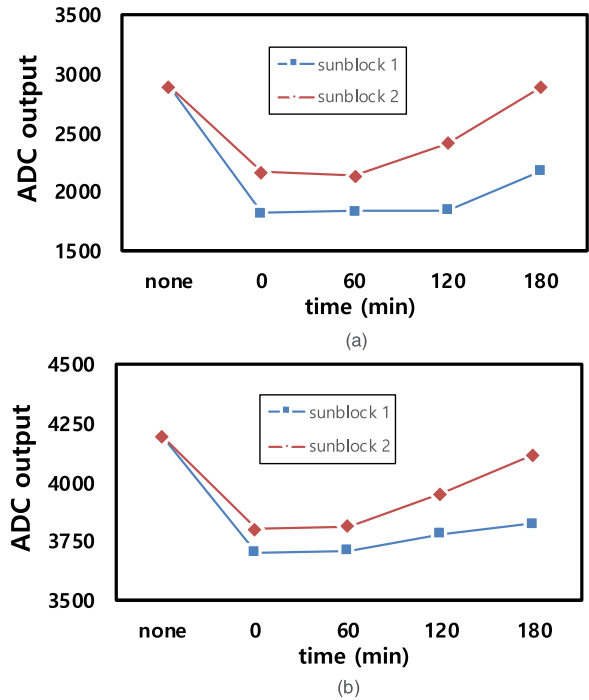

FIGURE 10. Measured Δ_{UV} over time after the application of two different sunblock products (product 1 with SPF 50+ and PA+ + + + and product 2 with SPF 50+ and PA+ + +): (a) measured Δ_{UVA}; (b) measured Δ_{UVB}.

Fig. 10(a) and (b) show the measured UV protection over time for Δ_{UVA} ($\Delta_{UVA1} + \Delta_{UVA2}$) and Δ_{UVB} ($\Delta_{UVB1} + \Delta_{UVB2}$), respectively. These curves indicate the summed results for the 2 × 6 PD array, excluding the peripheral pixels. Because the commercial sensor did not support the measurement of UV protection, only the experimental results for the proposed sensor are provided; the measured quantity is also expressed as a digital number (ADC output) rather than in a.u. A tunable light source (TLS260-250Q) was used to apply UV light with wavelengths of 300 nm (UV$_B$) and 360 nm (UV$_A$). As optical filters were not used, we blocked ambient light during the experiments. However, in actual applications, a separate UV-pass filter that allows all UV wavelengths to pass through it should be applied. This filter can be fabricated as a thin layer or can be coated onto the encapsulation layer. The experimental procedure employed is as follows. First, we applied the sunblock product to the skin. Second, we waited for a specific amount of time (0, 60, 120, and 180 min) until the specific moment when the sunblock on the skin was weakened. Third, the sensor was contacted with the skin for the transfer of residual sunblock. Fourth, the intensity of UV light penetrating the transferred sunblock was measured. The UV protection afforded by sunblock products is assessed based on two criteria: the sun protection factor (SPF), which indicates the degree of protection against UV$_B$, and the degree of protection against UV$_A$ (PA), which is indicated by the number of "+"s. In both cases, a higher value/number indicates better UV protection. In this experiment, we used two products: sunblock 1 with SPF 50+ and PA+ + + + and sunblock 2 with SPF 50+ and PA+ + +.
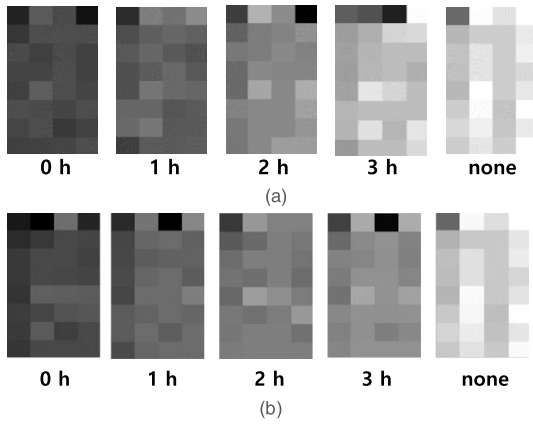
FIGURE 11. Captured UV images (Δ_{UVA} @ λ = 360 nm) for (a) sunblock 1; (b) sunblock 2.

FIGURE 12. Measured sebum levels for different oil volumes according to skin type: (a) dry skin; (b) oily skin.

FIGURE 13. Captured skin images over oil volume according to skin type.

TABLE 1. Chip characteristics.

	Process	110-nm CIS Process
	Core size	2.32×4.65 mm^2
	Pixel array	4×8
UV protection and sebum detection	PD area	3.6×3.6 µm^2
	Number of PDs/pixels	30×24
	UV responsivity	6.29 A/W (@ 350 nm)
	Visible light sensitivity/PD	448 mV/lx·s (@ 630 nm)
	Dark random noise	1.4 mV$_{rms}$
Hydration detection	Capacitance range	0–1 pF
	ADC resolution	9b
	ADC clock	600 kHz
	Supply voltage	1.5 V
	Power consumption	161.81 µW

Over time, the Δ-output increased owing to weakening of the sunblock. As shown in Fig. 10(a), the increase in the Δ-output for sunblock 1 was less than that for sunblock 2, owing to the superior UV$_A$ protection of the former. Sunblock 1 also offered better protection against UV$_B$, as shown in Fig. 10(b). Fig. 11 presents 4×8 UV images (@ 360-nm wavelength) for the two sunblock products that were used.

In this study, UV protection was detected under a fixed ambient illumination and a fixed position of the sensor; however, in practical applications, the sensor may generate different outputs depending on its position and the amount of incident light. In this prototype, we did not implement a calibration method to adjust the sensor output with respect to the incident illumination. Hence, in the future, a calibration method with separate photodetectors must be implemented for practical applications where UV protection needs to be detected or measured.

Fig. 12 depicts the sebum measured using side illumination from an external LED. In this experiment, we used a red LED with a wavelength of 637 nm. To detect light with this target wavelength, we also applied the Δ-readout, similar to that used for UV detection. The Δ-output of the PD array (with higher reset voltages than those for UV detection) was measured after the application of a skin oil. This experiment was performed on two persons: one with dry skin and another with oily skin. The application of additional oil to oily skin yielded a higher response (Δ-output). These experimental results are presented as 4×8 images in Fig. 13. We repeated the experiment with two commercial sensors [4], [7]. The proposed sensor afforded clearer discriminations of both oil contrast and skin type, as compared to the commercial sensor [7]. Although the commercial sensor [4] exhibited higher sensitivity, saturation occurred during the measurement of oily skin. The sensitivity of the proposed sensor can be enhanced by employing a microlens array (MLA) on the PD array such that additional photons are incident on the PDs. Although the MLA was not implemented in this prototype, it can be applied in the CMOS image sensor (CIS) process that was used for implementing the prototype sensor.
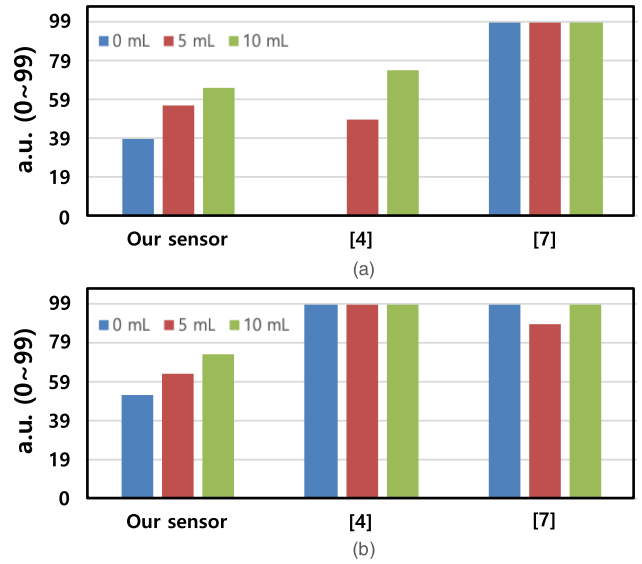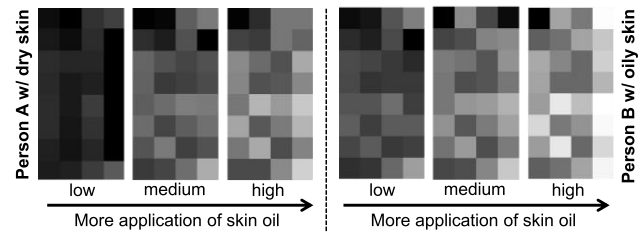
The chip characteristics are presented in Table 1. For a performance comparison, we used two commercial sensors [4], [7] and measured their sensitivity toward dehydration rate and sebum. The dehydration rate is represented by the average slope of the graph in Fig. 8, which indicates the sensitivity of hydration detection. Sebum sensitivity is represented by the average slope of the graph in Fig. 12. Compared to the commercial sensor, the proposed sensor exhibited a higher sensitivity toward the dehydration rate owing to the

TABLE 2. Performance comparison.

	Proposed sensor	[4]	[7]
Dehydration rate	0.25%/min	0.03%/min	0.05%/min
Sebum sensitivity over oil volume	2.32%/mL	3.75%/mL	0%/mL
UV-protection detection	Yes	No	No
Form factor	2.32×4.65 mm^2	$63 \times 53.6 \times 157.3$ mm^3	$10 \times 10 \times 130$ mm^3
Power consumption	161.81 μW	250 mW	-

strengthened e-field from an optimized IDC using the CMOS process. Moreover, the proposed sensor has a comparable sensitivity in detecting sebum. Although the sebum sensitivity of the commercial sensor [4] was higher, this sensor cannot detect oil contrast over oily skin because of its saturation, as shown in Fig. 12(b). Additionally, only the proposed sensor was capable of detecting UV protection. The two commercial sensors used in the experiments are assembled in a housing, whereas the proposed sensor is contained in a single chip. Therefore, a comparison of the form factor may be unfair. However, for complete comparison, information regarding the dimensions and power consumption of the sensors is presented in Table 2.

V. CONCLUSION

Herein, we present a single-chip CMOS skin sensor for detecting skin hydration, sebum, and UV protection. Pixels comprising IDCs stacked on a 30×24 PD array were used for area efficiency. These 4×8 skin pixels afford reliable detection regardless of the skin contact area and a high sensitivity, which was achieved via pixel merging. We implemented the spatiotemporal Δ-readout of PDs for the separate detection of UV$_A$ and UV$_B$. For the readouts of both IDCs and PDs, a column-parallel shared AFE and a 9b SAR ADC were integrated. Through experiments, it was determined that the proposed sensor exhibited higher sensitivity in detecting dehydration rate, sebum levels and UV protection, as compared to commercial sensors. Additionally, owing to the 110-nm CMOS process used, the sensor could be miniaturized to <9 mm^2, thereby enabling its integration onto a cotton pad for mobile skin diagnosis.

REFERENCES

[1] J. W. Fluhr, M. Gloor, S. Lazzerini, P. Kleesz, R. Grieshaber, and E. Berardesca, "Comparative study of five instruments measuring stratum corneum hydration (Corneometer CM 820 and CM 825, skicon 200, nova DPM 9003, DermaLab)—Part I. *In vitro*," *Skin Res. Technol.*, vol. 5, no. 3, pp. 161–170, Aug. 1999.

[2] J. W. Fluhr, M. Gloor, S. Lazzerini, P. Kleesz, R. Grieshaber, and E. Berardesca, "Comparative study of five instruments measuring stratum corneum hydration (Corneometer CM 820 and CM 825, skicon 200, nova DPM 9003, DermaLab)—Part II. *In vivo*," *Skin Res. Technol.*, vol. 5, no. 3, pp. 171–178, Aug. 1999.

[3] P. Clarys, R. Clijsen, J. Taeymans, and A. O. Barel, "Hydration measurements of the stratum corneum: Comparison between the capacitance method (digital version of the corneometer CM 825) and the impedance method (Skicon-200EX)," *Skin Res. Technol.*, vol. 18, no. 3, pp. 316–323, Aug. 2012.

[4] *MORITEX (moritex.com) Triplesense Datasheet*. Accessed: Jul. 20, 2020. [Online]. Available: http://moritex.com/products/upload/docs/Datasheet_Sensor.pdf

[5] *Delfin*. Accessed: Jul. 20, 2020. [Online]. Available: https://delfintech.com

[6] *Wayskin*. Accessed: Jul. 20, 2020. [Online]. Available: http://wayskin.com

[7] *Brrnoo Precision Skin Tester*. Accessed: Jul. 20, 2020. [Online]. Available: https://www.amazon.ca/Digital-Display-Precision-Moisture-nalyzer/

[8] S. Truong, "Design of a handheld skin moisture measuring device for application towards eczema," EE 4BI6 Elect. Eng. Biomed. Capstones, Dept. Elect. Comput. Eng., McMaster Univ., Hamilton, ON, Canada, 2009, Paper 15.

[9] B. Yang and Y. Dong, "A portable dual-parameter tester for assessing electrical properties of human skin surface," *IEEE Sensors J.*, vol. 16, no. 2, pp. 426–435, Jan. 2016.

[10] F. R. de Gruijl, "Skin cancer and solar UV radiation," *Eur. J. Cancer*, vol. 35, no. 14, pp. 2003–2009, Dec. 1999.

[11] D. G. Pitts, A. P. Cullen, and P. D. Hacker, "Ocular effects of ultraviolet radiation from 295 to 365 nm," *Invest. Ophthal. Vis. Sci.*, vol. 16, no. 10, pp. 932–939, 1977.

[12] M. Mazzillo, P. Shukla, R. Mallik, M. Kumar, R. Previti, G. Di Marco, A. Sciuto, R. A. Puglisi, and V. Raineri, "4H-SiC Schottky photodiode based demonstrator board for UV-index monitoring," *IEEE Sensors J.*, vol. 11, no. 2, pp. 377–381, Feb. 2011.

[13] J. J. Lee, S. Gandla, B. Lim, S. Kang, S. Kim, S. Lee, and S. Kim, "Alcohol-based highly conductive polymer for conformal nanocoatings on hydrophobic surfaces toward a highly sensitive and stable pressure sensor," *NPG Asia Mater.*, vol. 12, no. 1, pp. 1–10, Dec. 2020.

[14] J. Choi, S.-W. Han, S.-J. Kim, S.-I. Chang, and E. Yoon, "A spatial-temporal multiresolution CMOS image sensor with adaptive frame rates for tracking the moving objects in Region-of-Interest and suppressing motion blur," *IEEE J. Solid-State Circuits*, vol. 42, no. 12, pp. 2978–2989, Dec. 2007.

[15] S.-J. Kim, J. D. K. Kim, B. Kang, and K. Lee, "A CMOS image sensor based on unified pixel architecture with time-division multiplexing scheme for color and depth image acquisition," *IEEE J. Solid-State Circuits*, vol. 47, no. 11, pp. 2834–2845, Nov. 2012.

[16] A. Rush and P. Hubel, "X3 Sensor Characteristics," *J. Soc. Photogr. Sci. Technol. Japan.*, vol. 66, no. 1, pp. 57–60, 2003.

HYUNSUB NORBERT RIE (Member, IEEE) received the B.S. degree in semiconductor systems and engineering from Sungkyunkwan University, Suwon, South Korea, in 2018, and the M.S. degree in semiconductor and display engineering from Sungkyunkwan University.

He has been working at Samsung Electronics, Hwasung, since 2020. His research interests are analog circuit design and CMOS biosensors.

JUNHYUNG CHO (Member, IEEE) received the B.S. degree in electrical engineering from Kyunghee University, Suwon, South Korea, in 2018. He is currently pursuing the M.S. degree in electrical engineering with Sungkyunkwan University.

His research interests include analog circuit design and CMOS biosensors.

JUNGJOON LEE received the B.S. degree in chemical engineering from Kwangwoon University, Seoul, South Korea, in 2011, and the M.S. and Ph.D. (integrated course) degrees in chemical and biomolecular engineering from Yonsei University, Seoul, in 2016. He then worked at the Department of Intelligent Clean Materials, Korea Institute of Industrial Technology (KITECH), Cheonan, South Korea, in 2017. Since 2018, he has been working as a Postdoctoral Researcher with the Department of Advanced Material Science and Engineering, Sungkyunkwan University, Suwon, South Korea. His current research interests include highly conductive co-polymers and their application to flexible and stretchable electronic devices and sensors.

SRINIVAS GANDLA received the M.Sc. degree (applied electronics) from the Department of Physics, Osmania University, Telangana, India, in 2009, and the Ph.D. degree from the Department of Metallurgical Engineering and Materials Science, Indian Institute of Technology Bombay, India, in 2017.

He is currently a Postdoctoral Researcher with the School of Advanced Materials Science and Engineering, Sungkyunkwan University, Suwon, South Korea. His current areas of research include thin film transistors, and flexible and stretchable electronic devices and sensors.
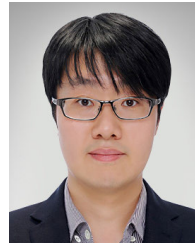
SEONG-JIN KIM (Member, IEEE) received the B.S. degree in electrical engineering from the Pohang University of Science and Technology, Pohang, South Korea, in 2001, and the M.S. and Ph.D. degrees in electrical engineering from KAIST, Daejeon, South Korea, in 2003 and 2008, respectively.

From 2008 to 2012, he was a Research Staff Member at the Samsung Advanced Institute of Technology, Yongin, South Korea, where he was involved in the development of a CMOS imager for the real-time acquisition of 3-D images. From 2012 to 2015, he was with the Institute of Microelectronics, A*STAR, Singapore, where he was involved in the design of analog-mixed signal circuits for various sensing systems. In 2015, he joined the School of Electrical and Computer Engineering, Ulsan National Institute of Science and Technology, Ulsan, South Korea, as an Assistant Professor. His current research interests include high performance imaging devices, and biomedical interface circuits and systems.

Dr. Kim currently serves on the Technical Program Committee at the IEEE International Solid-State Circuit Conferences since 2019.

JAEHYUK CHOI (Member, IEEE) received the B.S. degree in electrical engineering from Yonsei University, Seoul, South Korea, in 2004, the M.S. degree in electrical engineering and computer science from the Korea Advanced Institute of Science and Technology (KAIST), Daejeon, South Korea, in 2006, the M.S. degree in electrical and computer engineering from the University of Minnesota, Minneapolis, MN, USA, in 2008, and the Ph.D. degree from the University of Michigan, Ann Arbor, MI, USA, in 2013.

From 2013 to 2015, he was a Research Staff Member with the Samsung Advanced Institute of Technology (SAIT), Samsung Electronics, Suwon, South Korea, where he was engaged in researching depth sensors and low power image sensors. In 2015, he joined the Department of Semiconductor Systems Engineering, Sungkyunkwan University, Suwon, as an Assistant Professor. His research interests include low-power circuits, CMOS sensors, and mixed-signal integrated circuits.

· · ·